

Compton-thick active galactic nuclei inside local ultraluminous infrared galaxies

E. Nardini^{1,2*} and G. Risaliti^{2,3}

¹ *Dipartimento di Fisica e Astronomia - Sezione di Astronomia, Università di Firenze, L.go E. Fermi 2, 50125 Firenze, Italy*

² *INAF - Osservatorio Astrofisico di Arcetri, L.go E. Fermi 5, 50125 Firenze, Italy*

³ *Harvard-Smithsonian Center for Astrophysics, 60 Garden St., Cambridge, MA 02138 USA*

Released Xxxx Xxxxx XX

ABSTRACT

We present the X-ray analysis of the most luminous obscured active galactic nuclei (AGN) inside local ultraluminous infrared galaxies (ULIRGs). Our sample consists of ten sources, harbouring AGN components with estimated luminosity in excess of $\sim 10^{12} L_{\odot}$ and yet unidentified at optical wavelengths because of their large obscuration. According to the *Chandra* and *XMM-Newton* spectra, only in two cases out of ten clear AGN signatures are detected at 2–10 keV in the shape of reflected emission. The X-ray flux from the starburst (SB) components, instead, is always broadly consistent with the expectations based on their IR emission. The most convincing explanation for the missing AGN detections is therefore the Compton-thickness of the X-ray absorber. In general, the combination of our mid-IR and X-ray spectral analysis suggests that the environment surrounding the AGN component in ULIRGs is much richer in gas and dust than in ordinary active galaxies, and the degree of AGN absorption can be tentatively related to the SB intensity, indicating a strong interaction between the two processes and supporting the ULIRG/quasar evolutionary scheme.

Key words: galaxies: active; galaxies: starburst; infrared: galaxies; X-rays: galaxies.

* E-mail: nardini@arcetri.astro.it

1 INTRODUCTION

Accretion on to supermassive black holes (SMBHs) located in the centre of active galaxies provides a significant contribution to the energy irradiated over cosmic times. The spectral shape of the X-ray background and its progressive resolution into individual sources indicate that most active galactic nuclei (AGN) are heavily obscured by large column densities of dust and gas (e.g. Fabian & Iwasawa 1999; Gilli, Comastri & Hasinger 2007). According to the AGN unification model (Antonucci 1993), the differences observed in the optical spectra of AGN can be ascribed to the presence of a dusty torus surrounding the central engine: in nearly face-on objects, classified as type 1, favourable lines of sight allow the exploration of the very inner regions and the detection of broad emission lines on top of a strong optical/ultraviolet (UV) continuum. On the contrary, such spectral features are absent whenever the symmetry axis of the system lies close to the plane of the sky and the dusty screen blocks the direct nuclear light, so that only the high-ionization narrow lines originating from the outer regions are visible in type 2 objects as signatures of the underlying accretion activity. As the dust affects the optical spectral properties and classification, the amount of gas along the line of sight suppresses the X-ray emission through photoelectric absorption and Compton scattering. Compton-thick sources (i.e. those with $N_{\text{H}} \gtrsim 10^{24} \text{ cm}^{-2}$) are difficult to unveil at high redshift ($z \sim 1\text{--}3$) even with the deepest X-ray surveys (e.g. Alexander et al. 2003). None the less, the absorbed optical to soft X-ray primary radiation is reprocessed by the intervening material and re-emitted at longer wavelengths, driving a significant luminosity in the mid- and far-infrared (IR). Indeed, compelling evidence for the existence around $z \sim 2$ of a vast population of Compton-thick AGN among the IR galaxies has been found, by selecting through various criteria those sources showing excess mid-IR emission with respect to the predictions relative to the star formation component alone (Daddi et al. 2007; Fiore et al. 2008; Treister et al. 2009; Bauer et al. 2010).

The local counterparts of the IR systems harbouring the most obscured nuclear activity at high redshift are the so-called Ultraluminous infrared galaxies (ULIRGs, $L_{\text{IR}} \sim L_{\text{bol}} > 10^{12} L_{\odot}$), which rival optically-bright quasars as the most powerful sources in the nearby Universe with their huge mid- and far-IR emission, due to the dust reprocessing of higher-frequency radiation (Sanders & Mirabel 1996). It is now well-established that the hidden source of the primary radiation field inside ULIRGs is a combination of extreme star formation activity (starburst, SB) and highly obscured accretion, whose clear detection has

represented a long-standing challenge since the discovery of these objects (e.g. Genzel et al. 1998; Laurent et al. 2000). Therefore, two crucial points are to disentangle the AGN and SB components and to assess their contribution to the luminosity of both the individual sources and the local ULIRG population as a whole. These tasks are fundamental not only in order to understand the nature of local ULIRGs themselves, but also to shed light on the interplay and mutual feedback between star formation and BH accretion, which are basic ingredients of galaxy formation and evolution.

Taking advantage of the unprecedented data quality provided by the Infrared Spectrograph (IRS; Houck et al. 2004) onboard the *Spitzer Space Telescope* (Werner et al. 2004) we have recently developed an AGN/SB decomposition method for local ULIRGs based on 5–8 μm rest-frame spectroscopy (Nardini et al. 2008). The key physical motivation that prompts the selection of this narrow wavelength range for our analysis is the enhancement of the intrinsic AGN over SB brightness ratio (by a factor of ~ 10 – 50 ; Nardini et al. 2009, 2010) for equal bolometric luminosity, due to the intense emission from the hot dust layers exposed directly to the AGN. This enables the detection of even faint or heavily obscured AGN components that are missed at different wavelengths. Our spectral decomposition relies on a twofold observational evidence: at the highest luminosities the 5–8 μm average spectra of SB- and AGN-dominated sources are clearly different, and their dispersion is very limited (Brandl et al. 2006; Netzer et al. 2007). It is therefore possible to reproduce the AGN and SB contributions with fixed templates, only allowing for variable screen-like absorption of the AGN hot dust continuum occurring in the colder layers of the putative torus and/or in some dusty circumnuclear cloud.¹ Our main results can be summarized as follows:

1) The AGN detection rate among local ULIRGs is ~ 70 per cent, comparable to the amount achieved by collecting all the most effective multiwavelength diagnostics employed so far. Remarkably, this also matches the fraction of submillimetre galaxies (Alexander et al. 2005) and 70 μm -selected ULIRGs (Kartaltepe et al. 2010) hosting powerful AGN activity. However, 2) the main energy supply to the bolometric luminosity of such objects comes from star formation, with an average AGN/SB power balance of $\sim 1/3$. This ratio is confirmed to be luminosity-dependent, since the typical AGN contribution rises from ~ 10 to ~ 60 per cent across the ULIRG luminosity range. Consequently, the most intriguing outcome of our mid-IR analysis is 3) the identification in several sources of elusive AGN components missed

¹ A power-law extinction $\tau(\lambda) \propto \lambda^{-1.75}$ has been assumed (see also Draine 2003, and references therein).

by the standard optical diagnostic tools. In particular, we find that the sources characterized by a steep continuum (which in our model is interpreted as an effect of reddening), with deep absorption features and/or suppression of the polycyclic aromatic hydrocarbon (PAH) tracers of star formation, do not usually show the optical line ratios of active galaxies, and occasionally are classified as pure H II regions.

This subclass encompasses ~ 10 – 15 per cent of the local ULIRG population. Once corrected for extinction, some of these elusive AGN components account for most of the galaxy IR luminosity, falling in the quasar – rather than in the Seyfert – range. As a consequence, they represent the ideal targets for follow-up observations in the hard X-ray band, which are relevant to the quest for the most luminous, obscured AGN (i.e. type 2 quasars) in the local Universe, and can also give deeper insight into the physical properties and geometrical structure of the obscuring material in a ULIRG-like environment.

In this work we present the X-ray analysis of a sample of ten optically-elusive and IR-obscured AGN with quasar-like luminosity, which span a large range with respect to the relative AGN/SB contribution, the degree of AGN obscuration and the overall IR luminosity, and are therefore broadly representative of their parent class. New *Chandra* and *XMM-Newton* observations have been obtained for four of these objects, i.e. IRAS 00397–1312, IRAS 01003–2238, IRAS 01298–0744 and IRAS 12127–1412, while archival X-ray spectra are available for the other six buried AGN completing our sample. All the sources at issue are introduced in Section 2, with the log of the X-ray observations and a brief description of the data reduction. In Section 3 we discuss both the existing constraints and our new results on the sources of our X-ray sample, combining all these indications with our previous mid-IR analysis and interpreting them in the wider context of the connection between circumnuclear star formation and BH growth in Section 4. The conclusions are drawn in Section 5. Throughout this paper distances and luminosities have been computed assuming a Λ CDM cosmology based on the latest measures of the *Wilkinson Microwave Anisotropy Probe* ($H_0 = 70.5 \text{ km s}^{-1} \text{ Mpc}^{-1}$, $\Omega_m = 0.27$ and $\Omega_\Lambda = 0.73$; Hinshaw et al. 2009).

2 OBSERVATIONS AND DATA REDUCTION

In our previous work (Nardini et al. 2010) we have examined the 5 – $8 \mu\text{m}$ *Spitzer*-IRS spectra of 164 local ULIRGs at redshift $z \lesssim 0.35$, separating the AGN and SB components and providing a quantitative estimate of their contribution to the bolometric luminosity of each

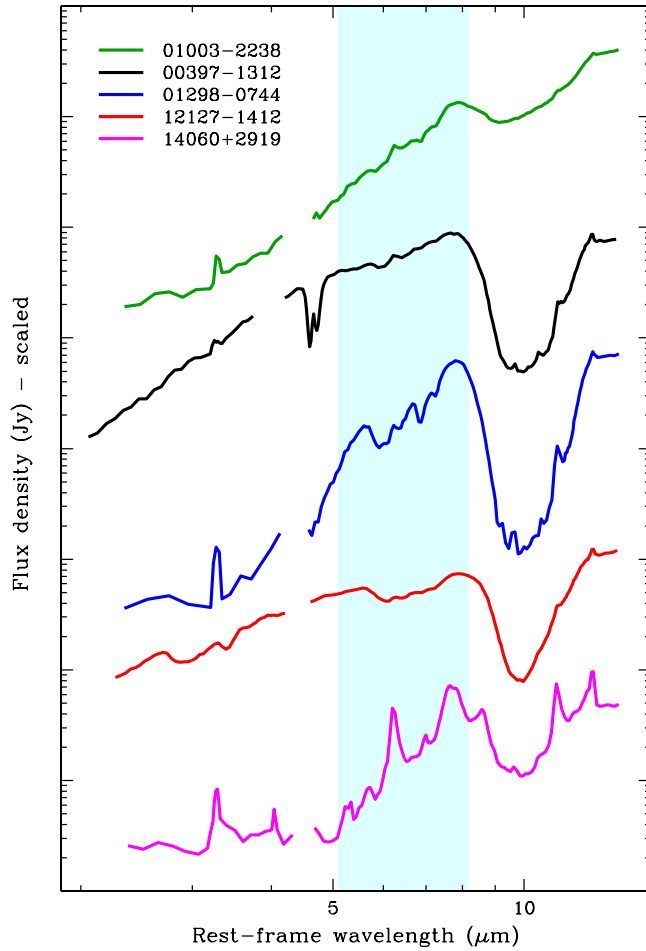


Figure 1. The $\sim 2\text{--}14\ \mu\text{m}$ rest-frame spectra (taken by *Akari* and *Spitzer*, and representative of the whole sample under study) of the four sources newly observed in the X-ray band. For the sake of comparison, we also show the spectrum of a typical SB-dominated ULIRG, IRAS 14060+2919. Each of our X-ray targets shows very faint or absent PAH emission (whose features are expected at 3.3, 6.2, 7.7, 8.6 and $11.3\ \mu\text{m}$) and broad formless and/or narrow deep absorption (due to e.g. water ice at ~ 3.1 and $6.0\ \mu\text{m}$, carbon monoxide at $4.65\ \mu\text{m}$, hydrogenated amorphous carbons at 6.85 and $7.25\ \mu\text{m}$, silicates at $9.7\ \mu\text{m}$). These are all signatures of the unambiguous presence of a buried compact engine and are not consistent with a SB-dominated environment. The shaded region indicates the interval used for our AGN/SB decomposition analysis. (The *Akari* spectra, courtesy of M. Imanishi, have been rebinned for display purpose.)

Table 1. General properties, IR spectral parameters and X-ray observation log of the sources selected for our X-ray analysis. (1) *IRAS* name, (2) redshift, (3) IR luminosity in log of solar units, (4) optical classification, (5) 1σ confidence range for the AGN bolometric contribution (in per cent) from our mid-IR analysis, (6) AGN optical depth at $6\ \mu\text{m}$, (7) X-ray satellite and observation identifier, (8) observation date, (9) net exposure in ks, (10) references.

Object (1)	z (2)	L_{IR} (3)	Type (4)	α_{bol} (5)	τ_6 (6)	ObsID (7)	Date (8)	T (9)	Ref. (10)
00091-0738	0.118	12.27 ± 0.03	H II	52-64	2.30	<i>Chandra</i> -10342	2008/11/01	15	4
00182-7112	0.327	12.95 ± 0.04	LINER	96-99	—	<i>XMM</i> -0147570101	2003/04/16	10	2
00397-1312	0.262	12.95 ± 0.08	H II	50-58	0.24	<i>Chandra</i> -11532	2009/08/23	44	1
01003-2238	0.118	12.33 ± 0.06	H II	46-54	1.58	<i>XMM</i> -0605880101	2009/12/08	28	1
01166-0844	0.118	12.12 ± 0.06	H II	78-94	2.35	<i>Chandra</i> -10344	2008/10/31	15	1
01298-0744	0.136	12.36 ± 0.05	H II	71-80	1.79	<i>Chandra</i> -11531	2009/10/21	21	1
07251-0248	0.088	12.41 ± 0.04	—	35-43	1.37	<i>Chandra</i> -7804	2006/12/01	15	1
08572+3915	0.058	12.15 ± 0.01	LINER	83-88	0.44	<i>Chandra</i> -6862	2006/01/26	14	3
11095-0738	0.107	12.28 ± 0.03	LINER	56-64	1.56	<i>Chandra</i> -10347	2009/04/09	16	4
12127-1412	0.133	12.20 ± 0.06	LINER	85-91	—	<i>Chandra</i> -11533	2010/04/30	35	1

References: ¹This work; ²Nandra & Iwasawa (2007); ³Teng et al. (2009); ⁴Teng & Veilleux(2010).

Table 2. Summary of the results of our X-ray spectral analysis.

Object	F_X^{AGN}	F_X^{SB}	F_X^{obs}	ϵ_{refl}
00091–0738	5.8	0.023	< 0.003	< 0.05
00182–7112	2.4	0.011	0.150	6.0
00397–1312	3.3	0.017	0.007	< 0.3
01003–2238	7.2	0.019	0.005	< 0.2
01166–0844	4.8	0.015	< 0.001	< 0.02
01298–0744	6.8	0.021	< 0.002	< 0.03
07251–0248	7.4	0.060	< 0.002	< 0.03
08572+3915	33	0.060	< 0.005	< 0.02
11095–0738	8.4	0.028	0.008	< 0.1
12127–1412	4.1	0.013	0.040	1.0

Note. F_X^{AGN} : intrinsic 2–10 keV AGN flux estimated from our mid-IR analysis, assuming standard SEDs and UV to X-ray corrections as described in the text; F_X^{SB} : upper limit to the 2–10 keV SB flux based on the average far-IR to X-ray relation for star-forming galaxies; F_X^{obs} : observed 2–10 keV flux; ϵ_{refl} : rough estimate of the AGN reflection efficiency (in per cent). All the fluxes are in units of 10^{-12} erg s $^{-1}$ cm $^{-2}$.

galaxy. This can be achieved by means of a straightforward analytical model, once the AGN emission has been corrected for cold dust extinction by using the reddening of the hot dust template as a measure of the optical depth (Nardini et al. 2008). It turns out that the optical classification is on average in good agreement with the findings of our mid-IR diagnostics. None the less, among the 20 ULIRGs (out of 164) for which we assess an AGN bolometric contribution (α_{bol}) larger than 25 per cent and an optical depth to the AGN (τ_6) larger than one at 6 μm , only three objects are optically classified as type 2 Seyferts. All the remaining entries are classified as either low-ionization nuclear emission-line regions (LINERs) or even H II regions, revealing that a substantial fraction of sources harbour significant but highly obscured nuclear activity.

We have therefore selected the optimal candidates for a supplementary spectral study of this population in the X-rays according to the following criteria, which are applied to the whole IR sample: 1) availability of a meaningful (i.e. > 5 ks exposure) X-ray observation;² 2) estimated AGN luminosity exceeding $\sim 10^{12} L_{\odot}$; 3) non-Seyfert optical classification (e.g. Veilleux, Kim & Sanders 1999). In particular, the second requirement removes any ambiguity in the AGN identification, since the nuclear component is always strong enough to dominate the 5–8 μm emission. The corresponding selection consists of six objects for which X-ray observations are already available, even if only in four cases the results have been published. Four additional sources, i.e. IRAS 00397–1312, IRAS 01003–2238, IRAS 01298–0744 and IRAS 12127–1412, all meeting the latter two criteria, have been obtained as a part of our

² The nature of the sources discussed in this work practically restricts the archival search to the present-day X-ray observatories, with large effective area at ~ 2 –10 keV. Even in this case, in fact, a non-detection in a very short snapshot would have a non-univocal interpretation.

X-ray follow-up campaign. They were chosen to complete the present sample, and for their remarkable expected X-ray properties:

(a) By assuming a standard quasar spectral energy distribution (SED; Elvis et al. 1994), suggesting that $\nu L_\nu(2500 \text{ \AA}) \simeq 2 \times \nu L_\nu(6 \text{ \mu m})$, and the most recent relations between the UV and X-ray luminosities (Lusso et al. 2010), the intrinsic 2–10 keV flux of the AGN component in IRAS 01003–2238 and IRAS 01298–0744 is expected to be $\sim 7 \times 10^{-12} \text{ erg s}^{-1} \text{ cm}^{-2}$, ensuring a prominent detection in case of a Compton-thin column density ($N_{\text{H}} \lesssim 5 \times 10^{23} \text{ cm}^{-2}$). Even in a Compton-thick prospect, allowing for a reflection efficiency of a few per cent makes the AGN clearly detectable with the current X-ray observatories.

(b) IRAS 00397–1312 and IRAS 12127–1412 are very interesting in this context as well (see also Imanishi et al. 2008, 2010). The former is optically classified as H II region in spite of being the most luminous ULIRG in the 1 Jy sample (Kim & Sanders 1998), with $L_{\text{IR}} \simeq 10^{13} L_\odot$: its mid-IR spectrum shows faint PAH features (Fig. 1), and clearly hints at the simultaneous presence of a buried AGN roughly comparable to the SB in terms of its IR energy output. The latter is found instead near the lower end of the ULIRG luminosity range, but its heavily absorbed continuum lacking any star formation signature implies an AGN-dominated nature. For these two sources the predicted X-ray flux is just slightly less than the estimate given above (by a factor of ~ 2).

The four ~ 2 – 14 \mu m rest-frame spectra are fully representative of this ULIRG subclass, and are shown in Fig. 1 in contrast with a typical SB template, while the general information concerning all the sources and their physical parameters as derived from our mid-IR analysis are listed in Table 1. Considering all the entries, this X-ray sample allows us to probe a wide range of properties with respect to obscured activity inside ULIRGs. It is also worth emphasizing that the 2–10 keV flux obtained by ascribing all the far-IR emission³ to the SB component and applying the far-IR to X-ray correlation of Ranalli, Comastri & Setti (2003) lies in the range ~ 1 – $6 \times 10^{-14} \text{ erg s}^{-1} \text{ cm}^{-2}$, which is on average ~ 300 times⁴ lower than what envisaged for the AGN (see Table 2). The median 2–10 keV luminosity predicted for the AGN component is $L_{\text{X}} \sim 2.5 \times 10^{44} \text{ erg s}^{-1}$. This is actually a conservative evaluation: if we adopt the direct 6 \mu m to 2–10 keV correction found by Lutz et al. (2004a), it should

³ We assume $F_{\text{FIR}} = 1.26 \times 10^{-11} (2.58 f_{60} + f_{100}) \text{ erg s}^{-1} \text{ cm}^{-2}$, where the *IRAS* flux densities f_{60} and f_{100} are in Jy (Helou, Soifer & Rowan-Robinson 1985).

⁴ We note that our absorption correction of the AGN flux is ~ 10 at most ($\tau_6 \simeq 2.35$ in IRAS 01166–0844), hence it does not significantly affect the contrast between the AGN and SB expected X-ray brightness.

be revised upwards by a factor of ~ 2 . This places our sources well above the X-ray intrinsic luminosity of the local population of Compton-thick AGN recently identified by Goulding et al. (2011), allowing us to explore the parameter space of highly obscured AGN in the low-redshift/high-luminosity region.

Concerning the unpublished X-ray data, IRAS 01003–2238 was observed by *XMM-Newton* on 2009 December 08 for 35 ks. The EPIC pn and MOS cameras operated in full frame mode. After the filtering of high-background periods, the useful pn exposure is ~ 28 ks. Incidentally, a previous snapshot (~ 10 ks) taken with *Chandra* in 2003 yielded only 20 counts at 0.5–8.0 keV, preventing a detailed spectral modelling (Teng et al. 2005). The other five sources, instead, were observed with the *Chandra* ACIS-S detector. The basic details about all the observations are summarized in Table 1. The data reduction was performed following the standard procedures, using the latest versions of the CIAO and SAS packages for *Chandra* and *XMM-Newton* event files, respectively. The source and background spectra were extracted from circular regions with radius of $2''$ (*Chandra*) and $30''$ (*XMM-Newton*). In each case the X-ray emission from the source is entirely collected within the chosen aperture, corresponding to ~ 3 – 10 kpc in the *Chandra* images. No clear morphological structure can be appreciated. The analysis has been performed on unbinned spectra using the XSPEC v12.5 fitting package, and C -statistic has been adopted due to the low number of counts. Quoted uncertainties and upper limits are given at the 90 per cent confidence level.

3 SPECTRAL ANALYSIS AND DISCUSSION

Since ULIRGs are in general very faint X-ray sources, only a limited number of objects in our local IR sample have been targeted with the current X-ray observatories *Chandra* (Ptak et al. 2003; Teng et al. 2005), *XMM-Newton* (Franceschini et al. 2003) and *Suzaku* (Teng et al. 2009). A compilation of all publicly available X-ray data for 40 ULIRGs has been recently discussed by Teng & Veilleux (2010).

Analogously to their mid-IR spectra, the X-ray spectra of ULIRGs usually show the combined signatures of AGN and SB activity; in particular, the soft ($E < 2$ keV) emission is characterized by a diffuse thermal component associated with star formation in the circumnuclear regions, while at higher energies the hard AGN power law is transmitted through typical column densities of the order of $\sim 10^{23}$ cm $^{-2}$. For Compton-thick sources a flat reflection spectrum is expected, alongside the prominent iron K line due to fluorescent emission in

the surrounding optically-thick and almost neutral gas (e.g. Matt, Brandt & Fabian 1996). In this section we first analyse our new observations and then review the existing X-ray spectra of the other elusive AGN in our sample, in order to explore the properties of the obscured AGN population within local ULIRGs and obtain some useful hints about and their high-redshift equivalents.

3.1 IRAS 00397–1312

As mentioned above, IRAS 00397–1312 is one of the most striking objects in the local Universe for many reasons. Owing to its huge luminosity and composite nature, it is an ideal source for a case study of the AGN/SB connection in extreme environments. This ULIRG does not show clear morphological indications of a recent interaction, and likely represents an old merger stage (Veilleux, Kim & Sanders 2002). Despite its optical classification as H II region, the mid-IR spectral shape reveals all the unambiguous signatures of a buried AGN (Imanishi 2009), first and foremost the outstanding CO absorption profile around $\sim 4.65 \mu\text{m}$. The X-ray spectrum of IRAS 00397–1312 is shown in Fig. 2: the only detected X-ray emission is well reproduced by means of an absorbed power law, resulting in a C -stat of 45.0 for 52 degrees of freedom (d.o.f.). Besides the Galactic column density along the line of sight towards the target, which has been taken into account in all our fits, an additional X-ray absorber with $N_{\text{H}} \simeq 4.5 \times 10^{21} \text{ cm}^{-2}$ local to the source at $z = 0.262$ is required. The unabsorbed 0.5–2 and 2–10 keV fluxes are, respectively, ~ 9 and $7 \times 10^{-15} \text{ erg s}^{-1} \text{ cm}^{-2}$, and are both in good agreement with the SB X-ray flux predicted from our mid-IR analysis and the Ranalli et al. (2003) relations for star-forming galaxies (Table 2). The steepness of the power law, whose photon index is $\Gamma \simeq 2.3_{-0.6}^{+1.1}$, is itself consistent with pure SB emission with no AGN contribution; for the latter, an upper limit has been evaluated by adding a PEXRAV component (Magdziarz & Zdziarski 1995) to account for possible AGN reflection. All the geometrical and abundance parameters have been frozen to their nominal PEXRAV values, as well as the photon index of the illuminating AGN power law (assumed to be 2.0). The upper limit to the observed 2–10 keV AGN flux is $\sim 7.6 \times 10^{-15} \text{ erg s}^{-1} \text{ cm}^{-2}$, implying a reflection efficiency < 0.3 per cent (Table 2), far below the usual values of ~ 1 –5 per cent. We will discuss this point further in the following. We note that the inclusion of a MEKAL component (i.e. emission from hot diffuse gas) improves the fit at soft energies, but makes

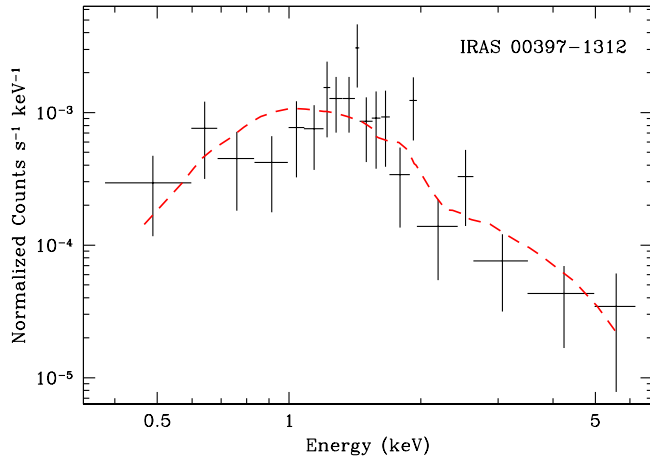


Figure 2. *Chandra* spectrum of IRAS 00397–1312 reproduced with a TBABS*ZWABS*POWERLAW model. In these figure and the following ones, the X-ray data are rebinned for plotting purposes.

the hard X-ray parameters badly constrained. Given the low quality of our data, we favour a simpler model even if the statistical significance is slightly lower.

3.2 IRAS 01003–2238

This source is usually classified as H II region in the optical (Veilleux et al. 1999), yet there are also some conflicting claims about its possible Seyfert 2 nature (Allen et al. 1991; Yuan, Kewley & Sanders 2010). Although detected, absorption features in the mid-IR are not dramatic in both depth and shape, and PAH emission is clearly distinguished on top of a very steep continuum. The X-ray spectrum is described with a power law plus a MEKAL component, yielding a C -stat/d.o.f. = 21.3/35. The spectrum is very soft (Fig. 3), and is characterized by a MEKAL temperature of $kT = 0.66^{+0.31}_{-0.21}$ keV and a power law photon index of $2.9^{+0.4}_{-0.3}$, suggesting again a sole SB origin. The observed flux is broadly consistent with such interpretation ($\sim 2 \times 10^{-14}$ and 5×10^{-15} erg s $^{-1}$ cm $^{-2}$ in the 0.5–2 and 2–10 keV energy range). An upper limit to the 2–10 keV AGN contribution has been computed as above, resulting in $\sim 1.3 \times 10^{-14}$ erg s $^{-1}$ cm $^{-2}$. Hence, similar considerations can be drawn in this case: no direct AGN emission is detected below 10 keV, hinting at a Compton-thick circumnuclear environment. The lack of any AGN signature even in the form of a reflected spectrum implies a complete covering of the X-ray absorber.

3.3 IRAS 01298–0744

This is undoubtedly the most puzzling object of the present selection, since the outcome of our X-ray observation is at first a striking non detection, as also confirmed with the

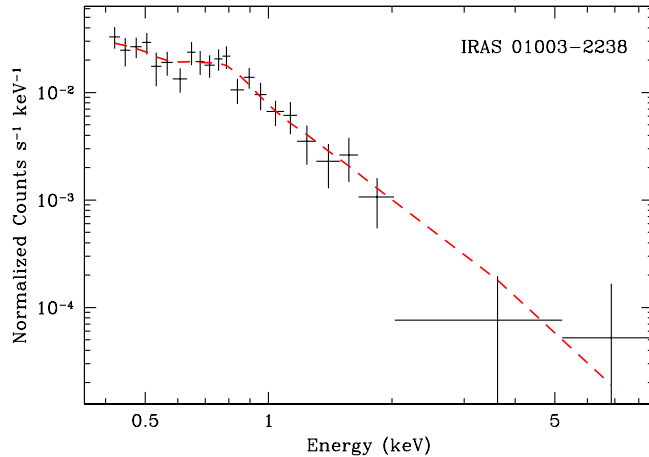


Figure 3. *XMM-Newton* spectrum of IRAS 01003–2238 and best fit obtained according to a TBABS*(MEKAL+POWERLAW) model. Only the EPIC pn data have been plotted.

CIAO ‘wavdetect’ tool. A serendipitous unidentified faint source is found $\sim 15''$ away from the ULIRG position, but any physical relation between the two can be ruled out since this angular distance is equivalent to over 30 kpc at the redshift of IRAS 01298–0744, which is actually an advanced merger with only residual tidal tails. By considering the background count rate, we can provide an upper limit to the observed 2–10 keV source excess of $\sim 2 \times 10^{-15}$ erg s $^{-1}$ cm $^{-2}$, corresponding to a marginal detection with 2σ confidence level. Such a limit is significantly lower than the related entries of Table 2, and yet reconcilable with a SB component with a far-IR luminosity of $\sim 2 \times 10^{11} L_{\odot}$, that would account for ~ 10 per cent of the overall IR emission. Ascribing instead the upper limit to an AGN with an intrinsic X-ray flux as that predicted, the resulting column density has to be larger than $\sim 8 \times 10^{24}$ cm $^{-2}$. As discussed in the following, this case is not unique in its class.

3.4 IRAS 12127–1412

IRAS 12127–1412 is one of the few objects in our large IR sample whose 5–8 μ m spectral shape cannot be reproduced by means of the standard AGN and SB templates. In fact, the observed emission is characterized by a broad formless absorption trough affecting most of the range of interest, and the putative continuum is slightly flatter than the assumed AGN hot dust component. This prevents us from measuring τ_6 from the reddening, and yet the AGN obscuration is likely to be substantial: first, because a stepwise correlation between the continuum reddening and the presence of individual absorption features is reasonably expected (e.g. Sani et al. 2008; Nardini et al. 2009); second, because the steeper trend seen shortwards of 5 μ m (Fig. 1) hints at a change in the slope of the extinction law (e.g.

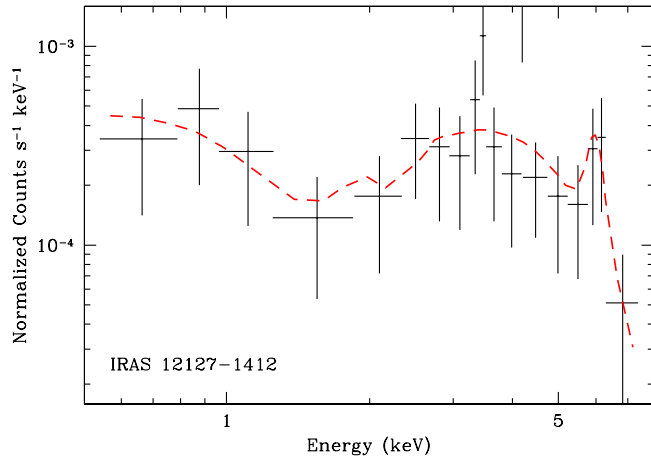


Figure 4. The complex X-ray emission of IRAS 12127–1412, modelled as $\text{TBABS}^*[\text{POWERLAW}+\text{ZWABS}^*(\text{ZGAUSS}+\text{POWERLAW})]$ with $C\text{-stat}/\text{d.o.f.} = 48.0/47$. The observed 2–10 keV flux and the detection of a prominent iron line clearly point to AGN reflection.

Nishiyama et al. 2009) rather than at vanishing obscuration. Based on these considerations, the intrinsic X-ray flux quoted in Section 2 for the AGN component of IRAS 12127–1412 can even be underestimated. It is therefore remarkable that the only clear AGN detection among our new observations unfolds in this source (Fig. 4). Indeed, the X-ray spectrum is quite complex: a steep power-law ($\Gamma \simeq 3.0 \pm 1.5$) or thermal component is needed at soft energies, while the hard emission can be modelled with a prominent iron feature at $\sim 6.77^{+0.50}_{-0.33}$ keV on top of an absorbed ($N_{\text{H}} \simeq 9^{+17}_{-5} \times 10^{22} \text{ cm}^{-2}$) continuum. All the parameters cannot be adequately constrained, but the characteristic flatness of a cold reflection spectrum is not observed, since the photon index of the AGN component is $\sim 2.0^{+1.1}_{-0.4}$. Also, the line energy is more consistent with He-like iron than with cold neutral material, pointing to ionized reflection. Unfortunately, we are not able to discuss this uncommon but intriguing scenario in detail. We simply note that such a possibility has already been suggested for IRAS 00182–7112, which is included in our X-ray sample as well and is remarkably similar to IRAS 12127–1412 both in the mid-IR and in the X-rays (Spoon et al. 2004; Nandra & Iwasawa 2007), as described below. Returning to the source at issue, we estimate an equivalent width for the K-shell feature of ~ 1.3 keV, with a lower limit that can be roughly placed at 0.4 keV.⁵ The observed flux in the 0.5–2 and 2–10 keV range is $\sim 2 \times 10^{-15}$ and $4 \times 10^{-14} \text{ erg s}^{-1} \text{ cm}^{-2}$, and adds further evidence to the presence of an obscured AGN with a reflection efficiency of ~ 1 per cent.

⁵ A rigorous calculation of the line parameters is precluded by the vanishing continuum at higher energies.

3.5 IRAS 01166–0844 and IRAS 07251–0248

Two other objects within our selection of ULIRGs that are missed by the optical diagnostics as Seyfert galaxies but likely harbour an AGN with quasar-like luminosity, although observed in the X-rays, have never been published to date. We have therefore reduced as outlined above and then analysed the ~ 15 ks long observations of IRAS 01166–0844 and IRAS 07251–0248 retrieved from the *Chandra* archives. The former source is a close equivalent (although much fainter) to IRAS 01298–0744 at $5\text{--}8\ \mu\text{m}$; strikingly, it turns out to be completely undetected as well. The latter, instead, which is a very bright source in the *IRAS* Revised Bright Galaxy Sample ($z \simeq 0.088$, $f_{60} \simeq 6.5$ Jy; Sanders et al. 2003) delivers a 3.5σ detection, and its weak emission can be fitted with a steep power law of photon index $\simeq 3.6(\pm 1.6)$. In both cases, the upper limit (or estimated) 2–10 keV flux is of the order of $\sim 10^{-15}$ erg s $^{-1}$ cm $^{-2}$. Assuming again the far-IR to X-ray conversion of Ranalli et al. (2003), such a tiny value implies not only that the AGN is thoroughly absorbed, but also that the SB provides very little contribution to the bolometric luminosity of the host galaxy.

3.6 The whole X-ray sample

The remaining four sources in our sample similarly display strong evidence for buried nuclear activity at mid-IR wavelengths, with spectral trends that are well represented by the ones shown in Fig. 1. At high energies, IRAS 00091–0738 and IRAS 11095–0238 have been classified as *weak* X-ray ULIRGs by Teng & Veilleux (2010): the small count rate does not allow traditional spectral fitting, and the only possible analysis is based on hardness ratio methods. We have reviewed these ~ 15 ks *Chandra* observations to obtain a measure of the received 2–10 keV flux, and found that it is consistent with a SB origin of only less than ~ 15 and 30 per cent, respectively, of the far-IR emission (see Table 2), assuming that no X-ray contribution from the AGN is detected.

Meaningful results have been obtained, instead, for the other two sources, which are definitely among the most extreme ULIRGs. IRAS 00182–7112, as already mentioned, is shown to harbour a Compton-thick AGN, with flat continuum and prominent Fe xxv $K\alpha$ emission; the reflection component itself is likely to be transmitted through a screen with $N_{\text{H}} \sim 10^{23}$ cm $^{-2}$ (Nandra & Iwasawa 2007). IRAS 08572+3915, instead, has been investigated with all the current X-ray observatories: it exclusively reveals a very marginal detection with *Chandra*, but no high-energy emission is seen with *Suzaku* (Teng et al. 2009). CO measurements imply

for this source a gas column up to $\sim 3 \times 10^{25} \text{ cm}^{-2}$ (Evans et al. 2002). As a consequence, both these galaxies can be considered as a template type 2 quasar in the local Universe.

Summarizing, the low number of counts collected from the elusive AGN in our present X-ray ULIRG sample is compatible with the Compton-thickness of the putative X-ray absorber, as well as the detection of iron lines with huge equivalent width, resembling the other notable case of Arp 220 (Iwasawa et al. 2005; Downes & Eckart 2007). In other words, virtually all ULIRGs with unambiguous mid-IR signatures of powerful, buried AGN activity are extinguished in the X-rays, with high incidence of Compton-thick objects and a wide gamut of reflection efficiencies, ranging from values expected for a standard type 2 obscuration geometry to much lower ones indicative of full and/or complex covering.

4 DISCUSSION

The X-ray observations analysed in this work provide further insight into the physical and geometrical properties of the gaseous material surrounding the AGN and responsible for its obscuration in a ULIRG environment. Assuming the validity of the Compton-thick scenario rather than invoking extremely unusual IR to X-ray corrections and/or X-ray reflection efficiencies, the missing AGN detections below 10 keV have two main implications which are tightly linked with each other, concerning the covering factor of the X-ray absorber and the coupling of the gas and dust components in the outskirts of the compact active source. Also, we discuss our results in the context of the AGN/SB connection, searching for possible relations between the excess of AGN obscuration and the strenght of the simultaneous burst of star formation.

4.1 The nature of the X-ray absorber

As pointed out earlier, the upper limits that can be placed on the possible AGN reflected emission imply a complete covering of the nuclear region. In the X-ray obscured AGN that are classified in the optical as type 2s, the direct optical to soft X-ray radiation blocked by the claimed axisymmetric dusty absorber can be scattered into the line of sight after the interactions with material located above the equatorial plane. This process strongly affects the shape of the emerging spectrum in the X-rays, and the usual efficiency in terms of the received flux is of the order of a few per cent, depending on geometrical effects. Except for the two AGN detections, in all the other sources of our sample we assess a reflection effi-

ciency lower than $\sim 2 \times 10^{-3}$, assuming an intrinsic 2–10 keV flux consistent with the results of the mid-IR analysis. Thus, regardless of the large and manifold uncertainties involved in the single cases, the X-ray follow-up observations of buried AGN presented or reviewed here generally hint at a cocoon-like geometry of the absorber, which is not surprising in extreme and chaotic systems such as ULIRGs.

Indeed, the detection of so prominent CO gas absorption in objects like IRAS 00182–7112 (Spoon et al. 2004) and IRAS 00397–1312 could be related with full covering rather than toroidal obscuration, since this feature is not usually found among type 2 Seyferts (e.g. Lutz et al. 2004b). As a consequence, the most interesting aspect to investigate concerns the location of the absorber and the properties of its gas and dust content. By adopting a typical Galactic extinction curve (e.g. Draine 2003; Nishiyama 2008, 2009) and the standard Galactic dust-to-gas ratio (Bohlin, Savage & Drake 1978), one can easily obtain the relation between the optical depth at 6 μm and the X-ray column density, that is $N_{\text{H}} \simeq 8\text{--}11 \tau_6 \times 10^{22} \text{ cm}^{-2}$. Then, even questioning the accuracy of our measure, any reasonable value of the *real* τ_6 would not be consistent with a Compton-thick environment with dust and gas components similar to the Galactic diffuse interstellar medium. The ensuing point is whether the X-ray column density is physically related to the dust affecting the optical and mid-IR diagnostics. There is plenty of observational evidence indicating *anomalous* dust properties in AGN for which different explanations have been proposed. For instance, X-ray absorption may occur in the very inner regions, inside the dust sublimation radius (e.g. Granato, Danese & Franceschini 1997); conversely, the formation of large dust grains favoured by high density environments yields a flat extinction curve misleading about the actual dust-to-gas ratio (Maiolino, Marconi & Oliva 2001).

In ULIRGs the situation is even more complex: a remarkable example is represented by Mrk 231, a bright ULIRG which is optically classified as a *Broad Absorption Line* quasar, and whose fairly unabsorbed *Spitzer*-IRS spectrum suggests a relative AGN contribution to the bolometric luminosity of the galaxy of ~ 30 per cent at least. The 2–10 keV emission of Mrk 231 reveals a reflection component only (Gallagher et al. 2002), while the direct AGN continuum shows up at 15–60 keV in the *BeppoSAX* data (Braitto et al. 2004). This mismatch between the optical and X-ray classification based on the obscuration degree in each band is not infrequent, and suggests a scarce gas/dust coupling around the AGN. Moreover, the case of Mrk 231 is indicative of the incidence of outflows: massive gas inflows are needed to sustain nuclear accretion, yet the possible link of the X-ray absorbing gas with AGN-

driven winds and outflows has far-reaching implications in terms of the AGN feedback and the ULIRG/quasar evolutionary pattern. According to this scenario, ULIRGs (or at least a significant fraction of them) are a transitory phase of galactic lifetime preliminary to the optically-bright quasar stage, during which the merger-driven inflows provide the gas reservoir for starburst and buried nuclear activity, until the AGN feedback disrupts the obscuring shell of dust and gas, quenching the circumnuclear star formation and sweeping the line of sight to the optical quasar (Sanders et al. 1988; Hopkins et al. 2008).

AGN- or SB-driven galactic winds are known to play a key role in the evolution of galaxies and are found in most ULIRGs (Veilleux, Cecil & Bland-Hawthorn 2005, and references therein). Unambiguous evidence for gas outflows has been recently discovered in the mid-IR also in buried AGN candidates. High-resolution *Spitzer*-IRS spectra reveal the presence of high-velocity gas in IRAS 00182–7112, giving rise to a broad component in the [Ne II] and [Ne III] lines at 12.81 and 15.56 μm (Spoon et al. 2009). In both cases the line profile is asymmetric due to a blue wing. A similar behaviour is not observed in optical or near-IR forbidden lines, as a result of the large extinction. This blueshift is interpreted as the signature of the ongoing breaching of the obscuring medium surrounding the active nucleus. Only two other sources exhibit such an asymmetry in neon profiles: our target IRAS 12127–1412, and IRAS 13451+1232. The latter is also detected in [Ne V] at 14.32 μm , which is a straightforward tracer of the AGN radiation field due to the high ionization energy required (97.1 eV). This strongly blueshifted detection indicates a more advanced stage of this source in the process of cleaning its line of sight, which is consistent with its type 2 Seyfert classification in the optical. The larger part of ULIRGs with [Ne V] emission show a blueshift, and the higher the neon ionization state the larger the blueshift, proving that the speed of the outflow decreases with the distance from the ionizing core (Spoon & Holt 2009). In some cases the gas kinematics traced by neon lines can be associated with the expansion of radio jets. Anyway, out of 25 ULIRGs with either [Ne III] or [Ne V] blueshifted lines, 21 are optically-identified AGN.⁶ IRAS 00182–7112, IRAS 12127–1412 and IRAS 01003–2238 (neglecting its controversial classification) are among the few exceptions. In this picture, mid-IR buried and X-ray Compton-thick AGN are still fully enshrouded, and their feedback is not yet in action.

⁶ Most of these sources are also included in our IR sample.

4.2 AGN feedback and SB intensity

On the wake of the considerations above, it is worth investigating the possible relation between the AGN mid-IR obscuration and the SB intensity. Fierce star formation activity is ubiquitous in AGN both in the local Universe (Schweitzer et al. 2006) and at high redshift (Hatziminaoglou et al. 2010). Moreover, far-IR observations suggest that X-ray absorbed AGN suffer a larger contamination from the concurrent star formation than unabsorbed ones at the same luminosity and redshift (e.g. Stevens et al. 2005). In order to address this issue, we have plotted in Fig. 5 the luminosities of the AGN and SB components derived from our mid-IR spectral decomposition, with a code emphasizing the degree of AGN extinction at $6\ \mu\text{m}$. The relative contribution is indicated by the diagonal lines, which follow the AGN *weight* classification defined in Nardini et al. (2010). Before drawing some qualitative considerations, we stress that the exact location of each ULIRG in this plot is affected by several sources of systematic uncertainty. In fact, α_{bol} [here simply given by $(1 + L_{\text{SB}}/L_{\text{AGN}})^{-1}$] is an absorption-corrected quantity and was calculated as a function of the intrinsic AGN and SB bolometric corrections averaged over the whole sample, but their *actual* values for the single objects can be quite different.⁷ Also, any deviation from the assumed templates and extinction law will modify both τ_6 and α_{bol} , and the difference in the merger stage does not allow a uniform interpretation. This notwithstanding, at the higher AGN luminosities (i.e. above $L_{\text{AGN}} \approx 10^{12} L_{\odot}$), where all the entries of our X-ray sample lie and the mentioned *confusion* effects should be less important, the intensity of the concurrent SB activity seems to be loosely correlated to the AGN mid-IR obscuration. Similarly, in terms of growing α_{bol} , when the AGN is still obscured the SB can be very powerful, accounting for roughly half of the total luminosity, but the production of stars subsides when the line of sight is clean.

At a more speculative level, we focus on the three ULIRGs that have an *anomalous* 5–8 μm spectral shape with flat but deeply absorbed continuum, and are clearly AGN-dominated in the mid-IR. These are the magenta stars in the top left-hand corner of Fig. 5, i.e. IRAS 00182–7112, IRAS 12127–1412 and IRAS 12514+1027. It turns out that all of them are detected as reflected AGN emission in the hard X-rays (see Wilman et al. 2003 for the latter object, not included in the present sample). This intriguing case hints at the possibility of distinguishing through mid-IR analysis only between a Compton-thickness associated

⁷ The 1σ dispersion inherent in our method is ~ 0.18 dex (see Nardini et al. 2009, 2010 for a review and a comprehensive discussion of our IR analysis).

to a toroidal X-ray absorber and a Compton-thickness due to a complete AGN covering, coeval with the peak of SB activity. In the former scenario, one can argue that the X-ray reflection signatures arise from the inner edge of a slightly tilted torus with little opening angle; this would also imply direct access to a certain fraction of hot dust, possibly resulting in a flattening of the continuum in agreement with the spectral trends of quasars around $\sim 5 \mu\text{m}$ (see Netzer et al. 2007, and our discussion on the AGN template in Nardini et al. 2009). However, further observations are needed to test this conjecture and the chance, if any, to infer the X-ray column density and covering factor exclusively from IR diagnostics; this would be relevant to the study of IR galaxies at high redshift and to the measure of the contribution to the X-ray background from type 2 quasars.

Incidentally, we finally note that by extrapolating the fraction of absorbed AGN in Fig. 5 below $\alpha_{\text{bol}} = 0.05$, it looks possible that almost every ULIRG in the local Universe is the seat of nuclear activity, and that also some of the pure SB/ULIRGs (mostly falling outside the plotted region and representing ~ 30 per cent of the total ULIRG population) harbour an AGN which is both intrinsically faint and heavily obscured.⁸ In this perspective, the clear cut in the presence of absorbed sources at $\alpha_{\text{bol}} < 0.05$ is simply due to selection effects: first, when the SB dominates at even $5\text{--}8 \mu\text{m}$, the AGN optical depth can be underestimated, and some of the green dots would turn into red circles with just a tiny displacement; second, some of the non-detections would be shifted upwards, entering the plotted portion of the $\alpha_{\text{bol}} < 0.05$ region as either red circles or blue crosses.

5 CONCLUSIONS

Our recent mid-IR diagnostic campaign on local ULIRGs has revealed the presence in a sizable fraction of these sources of powerful AGN components, providing a significant contribution to the total energy output but missed at optical wavelengths because of their heavy obscuration. The mid-IR spectra of these intriguing sources provide strong evidence of buried nuclear activity, in the shape of a steep and intense continuum, dramatic suppression of PAH features and various absorption. In order to pursue a more exhaustive study of the extreme environment surrounding the AGN component inside this subclass of ULIRGs, we have presented the X-ray analysis of a representative sample consisting of ten objects of this kind, and

⁸ Such AGN components would be totally missed even with our method, because their contribution to the observed mid-IR spectra is too small: in our scheme, these objects are classified as pure SB/ULIRGs.

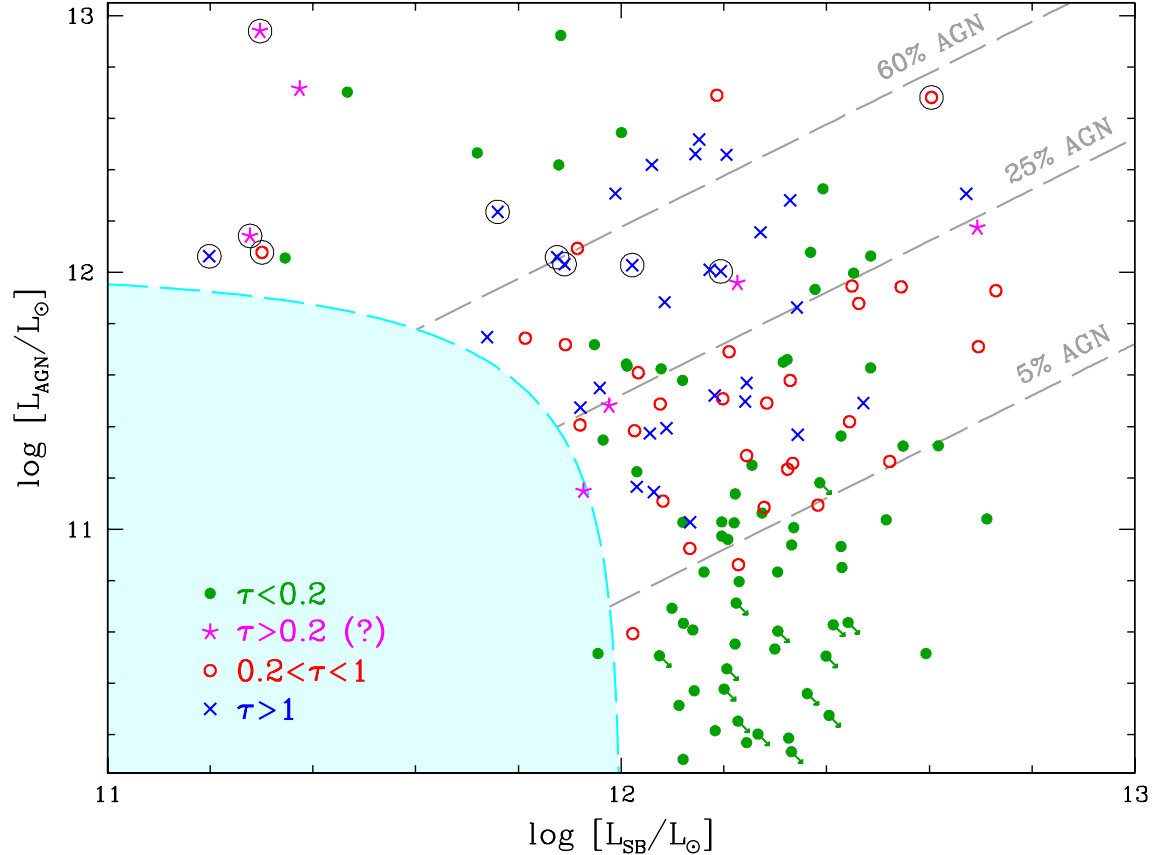


Figure 5. AGN versus SB luminosity from our mid-IR analysis. Different colours and symbols are used to distinguish the different estimates of the AGN optical depth at $6\ \mu\text{m}$. The magenta stars represent those ULIRGs with flat but heavily absorbed $5\text{--}8\ \mu\text{m}$ spectra, for which the continuum reddening cannot be used to measure the AGN optical depth. Interestingly, the largest X-ray reflection efficiencies for buried AGN are found among these objects. The cyan curve describes the boundary of our ULIRG sample, $L_{\text{IR}} = L_{\text{AGN}} + L_{\text{SB}} > 10^{12} L_{\odot}$ (all the sources meet this condition within the error bars, not shown), while the dashed diagonal lines trace the four regions of the α_{bol} space defined in Nardini et al. (2010). Most of the pure SB/ULIRGs lie outside the plot due to their low upper limit to L_{AGN} . Conversely, when the AGN is dominant, the degree of AGN obscuration in the mid-IR seems to be loosely related to the intensity of the concurrent star formation. Anyway, since each entry can be somewhat displaced due to the various sources of uncertainty (see the text), this plot is only intended for qualitative considerations (consequently, purely statistical error bars are omitted for clarity). The encircled objects are the ten ULIRGs presented or reviewed here.

including our new follow-up X-ray observations obtained with *Chandra* and *XMM-Newton* of IRAS 00397–1312, IRAS 01003–2238, IRAS 01298–0744 and IRAS 12127–1412. Only in IRAS 12127–1412 the presence of the AGN is clearly established in the X-rays, while IRAS 01298–0744 is not detected at all. The faint X-ray emission of IRAS 00397–1312 and IRAS 01003–2238 is consistent with a pure SB contribution, in terms of both spectral shape and observed flux. The other six sources in our X-ray sample, two of which have not been published to date, fully validate this general trend, with only another safe AGN detection in IRAS 00182–7112.

The main implications of this work are the following: 1) Assuming a typical dust extinction law, the dust-to-gas ratio is required to be much lower than the Galactic standard in order to support the Compton-thick interpretation for the unsuccessful AGN detections.

Of course, this is not due to a large-scale dust deficiency, since ULIRGs are, by definition, dust-rich systems. Anyway, absorption features such as that of CO at $4.65 \mu\text{m}$ observed in IRAS 00397–1312 hint at large amounts of gas concentrated nearby a compact active core. A possible imbalance between the dust and gas components involving only the nuclear regions (i.e. within a region comparable in size with the dust sublimation radius) may be related to massive gaseous inflows/outflows during the most active phases of AGN accretion.

2) Whenever the AGN is not detected but the amplitude of a possible reflection component can be constrained, its upper limit is > 500 times lower than the expected intrinsic 2–10 keV AGN flux. This is an order of magnitude lower than the usual reflection efficiency observed in type 2 active galaxies, suggesting an almost complete AGN covering in these ULIRGs. It is unlikely that the standard toroidal geometry of the dust absorber predicted for isolated and morphologically quiet AGN will hold systematically also for much more complex systems like ULIRGs, whose geometrical structure can be poorly retraced. Again, a complete covering is compatible with a spherical shell of gas infalling on to the accreting SMBH or, more conceivable in advanced merger stages, with the dust-free base of the winds invoked in the feedback scenario to clean the line of sight to the AGN and, possibly, to quench star formation.

The elusive AGN identified through their mid-IR spectral properties, the most notable of which have been discussed in this work, are likely going through the ultimate phase of buried activity, and are therefore the ideal sources to search for detectable signatures of the impending transition from ULIRGs to optically bright quasars. Even if the quality of the single X-ray spectra is very modest, the availability of X-ray constraints is crucial to derive a comprehensive multiwavelength picture. Extending the number of intrinsically luminous but heavily obscured AGN for which it is possible to infer the amount and distribution of gas in the circumnuclear environment and to compare such information with the optical to mid-IR dust extinction and absorption features and the intensity of the concurrent star formation may shed light on the ULIRG/quasar evolutionary sequence and the AGN feedback mechanisms affecting the properties of the host galaxy. Moreover, if the tentative correlation between mid-IR spectral properties and X-ray column density and covering factor is confirmed and clearly established, a simple *qualitative* inspection of the mid-IR spectra of the high-redshift counterparts of local ULIRGs will unveil Compton-thick AGN candidates and enable a measure of their contribution to the X-ray background.

ACKNOWLEDGMENTS

This research has been partially supported by NASA grants NNX09AT10G and GO0-11017X. We thank the anonymous referee for his/her constructive comments which improved our work.

REFERENCES

- Alexander D. M., et al., 2003, *AJ*, 126, 539
- Alexander D. M., Bauer F. E., Chapman S. C., Smail I., Blain A. W., Brandt W. N., Ivison R. J., 2005, *ApJ*, 632, 736
- Allen D. A., Norris R. P., Meadows V. S., Roche P. F., 1991, *MNRAS*, 248, 528
- Antonucci R., 1993, *ARA&A*, 31, 473
- Bauer F. E., Yan L., Sajina A., Alexander D. M., 2010, *ApJ*, 710, 212
- Bohlin R. C., Savage B. D., Drake J. F., 1978, *ApJ*, 224, 132
- Braitto V., et al., 2004, *A&A*, 420, 79
- Brandl B. R., et al., 2006, *ApJ*, 653, 1129
- Daddi E., et al., 2007, *ApJ*, 670, 173
- Downes D., Eckart A., 2007, *A&A*, 468, L57
- Draine B. T., 2003, *ARA&A*, 41, 241
- Elvis M., et al., 1994, *ApJS*, 95, 1
- Evans A. S., Mazzarella J. M., Surace J. A., Sanders D. B., 2002, *ApJ*, 580, 749
- Fabian A. C., Iwasawa K., 1999, *MNRAS*, 303, L34
- Fiore F., et al., 2008, *ApJ*, 672, 94
- Franceschini A., et al., 2003, *MNRAS*, 343, 1181
- Gallagher S. C., Brandt W. N., Chartas G., Garmire G. P., Sambruna R. M., 2002, *ApJ*, 569, 655
- Genzel R., et al., 1998, *ApJ*, 498, 579
- Gilli R., Comastri A., Hasinger G., 2007, *A&A*, 463, 79
- Goulding A. D., Alexander D. M., Mullaney J. R., Gelbord J. M., Hickox R. C., Ward M., Watson M. G., 2011, *MNRAS*, 411, 1231
- Granato G. L., Danese L., Franceschini A., 1997, *ApJ*, 486, 147
- Hatziminaoglou E., et al., 2010, *A&A*, 518, L33
- Helou G., Soifer B. T., Rowan-Robinson M., 1985, *ApJ*, 298, L7
- Hinshaw G., et al., 2009, *ApJS*, 180, 225
- Hopkins P. F., Hernquist L., Cox T. J., Kereš D., 2008, *ApJS*, 175, 356
- Houck J. R., et al., 2004, *ApJS*, 154, 18
- Kartalpe J. S., et al., 2010, *ApJ*, 709, 572
- Kim D.-C., Sanders D. B., 1998, *ApJS*, 119, 41
- Imanishi M., 2009, *ApJ*, 694, 751
- Imanishi M., Nakagawa T., Ohyama Y., Shirahata M., Wada T., Onaka T., Oi N., 2008, *PASJ*, 60, 489
- Imanishi M., Nakagawa T., Shirahata M., Ohyama Y., Onaka T., 2010, *ApJ*, 721, 1233
- Iwasawa K., Sanders D. B., Evans A. S., Trentham N., Miniutti G., Spoon H. W. W., 2005, *MNRAS*, 357, 565
- Laurent O., Mirabel I. F., Charmandaris V., Gallais P., Madden S. C., Sauvage M., Vigroux L., Cesarsky C., 2000, *A&A*, 359, 887
- Lusso E., et al., 2010, *A&A*, 512, A34

- Lutz D., Maiolino R., Spoon H. W. W., Moorwood A. F. M., 2004b, *A&A*, 418, 465
- Lutz D., Sturm E., Genzel R., Spoon H. W. W., Stacey G. J., 2004a, *A&A*, 426, L5
- Magdziarz P., Zdziarski A. A., 1995, *MNRAS*, 273, 837
- Maiolino R., Marconi A., Oliva E., 2001, *A&A*, 365, 37
- Matt G., Brandt W. N., Fabian A. C., 1996, *MNRAS*, 280, 823
- Nandra K., Iwasawa K., 2007, *MNRAS*, 382, L1
- Nardini E., Risaliti G., Salvati M., Sani E., Imanishi M., Marconi A., Maiolino R., 2008, *MNRAS*, 385, L130
- Nardini E., Risaliti G., Salvati M., Sani E., Watabe Y., Marconi A., Maiolino R., 2009, *MNRAS*, 399, 1373
- Nardini E., Risaliti G., Watabe Y., Salvati M., Sani E., 2010, *MNRAS*, 405, 2505
- Netzer H., et al., 2007, *ApJ*, 666, 806
- Nishiyama S., Nagata T., Tamura M., Kandori R., Hatano H., Sato S., Sugitani K., 2008, *ApJ*, 680, 1174
- Nishiyama S., Tamura M., Hatano H., Kato D., Tanabé T., Sugitani K., Nagata T., 2009, *ApJ*, 696, 1407
- Ptak A., Heckman T., Levenson N. A., Weaver K., Strickland D., 2003, *ApJ*, 592, 782
- Ranalli P., Comastri A., Setti G., 2003, *A&A*, 399, 39
- Risaliti G., Gilli R., Maiolino R., Salvati M., 2000, *A&A*, 357, 13
- Sanders D. B., Mirabel I. F., 1996, *ARA&A*, 34, 749
- Sanders D. B., Soifer B. T., Elias J. H., Neugebauer G., Matthews K., 1988, *ApJ*, 328, L35
- Sanders D. B., Mazzarella J. M., Kim D.-C., Surace J. A., Soifer B. T., 2003, *AJ*, 126, 1607
- Sani E., et al., 2008, *ApJ*, 675, 96
- Schweitzer M., et al., 2006, *ApJ*, 649, 79
- Spoon H. W. W., Holt J., 2009, *ApJ*, 702, L42
- Spoon H. W. W., et al., 2004, *ApJS*, 154, 184
- Spoon H. W. W., Armus L., Marshall J. A., Bernard-Salas J., Farrah D., Charmandaris V., Kent B. R., 2009, *ApJ*, 693, 1223
- Stevens J. A., Page M. J., Ivison R. J., Carrera F. J., Mittaz J. P. D., Smail I., McHardy I. M., 2005, *MNRAS*, 360, 610
- Teng S. H., Veilleux S., 2010, *ApJ*, 725, 1848
- Teng S. H., Wilson A. S., Veilleux S., Young A. J., Sanders D. B., Nagar N. M., 2005, *ApJ*, 633, 664
- Teng S. H., et al., 2009, *ApJ*, 691, 261
- Treister E., et al., 2009, *ApJ*, 706, 535
- Veilleux S., Kim D.-C., Sanders D. B., 1999, *ApJ*, 522, 113
- Veilleux S., Kim D.-C., Sanders D. B., 2002, *ApJS*, 143, 315
- Veilleux S., Cecil G., Bland-Hawthorn J., 2005, *ARA&A*, 43, 769
- Werner M. W., et al., 2004, *ApJS*, 154, 1
- Wilman R. J., Fabian A. C., Crawford C. S., Cutri R. M., 2003, *MNRAS*, 338, L19
- Yuan T.-T., Kewley L. J., Sanders D. B., 2010, *ApJ*, 709, 884